Electrochimica Acta 160 (2015) 363–375

Contents lists available at ScienceDirect

Electrochimica Acta

journal homepage: www.elsevier.com/locate/electacta

Irreversibility in redox molecular conduction: single versus double metal-molecule interfaces

Agostino Migliore [a,b,*], Abraham Nitzan [a]

[a] School of Chemistry, Tel Aviv University, Tel Aviv 69978, Israel
[b] Department of Chemistry, Duke University, Durham, NC 27708, USA

ARTICLE INFO

Article history:
Received 14 October 2014
Received in revised form 23 January 2015
Accepted 26 January 2015
Available online 29 January 2015

Keywords:
cyclic voltammetry
molecular conduction junctions
metal-molecule interfaces
charge transport
hysteresis

ABSTRACT

In this work we analyze the onset and manifestation of irreversibility phenomena in the charge transport at single and double metal-redox molecule interfaces, with special emphasis on the role of the nuclear system reorganization energy in causing the distortion of cyclic voltammograms in the first case and the occurrence of hysteresis phenomena in the second case. Under physical conditions for which two states of the molecular system come into play, effects of irreversibility increase with the reorganization energy at a single interface, while an opposite trend is seen in the conduction through a molecular junction. The apparent contradiction between these two behaviors, which was raised in a previous work (Migliore, A.; Nitzan, A., *J. Am. Chem. Soc.* 2013, *135*, 9420–32) is here resolved through detailed investigation of the connections between molecule reorganization energy, bias-dependent population of the molecular redox site(s), and threshold voltage scan rate for the onset of irreversible behavior. Moreover, our investigation of the effects of the reorganization energy on the voltammogram peaks proposes a strategy for extracting the value of the reorganization energy of the molecular system from the experimental behavior.

1. Introduction

Redox molecules have been subject of intensive and extensive experimental investigations in the last few decades, with special focus on electrochemical measurements that are able to detect their properties as systems of biological relevance [1–4] and of great potential in nano-electronics applications [2,5–9]. Properties such as reorganization energy of the redox molecular system and relative alignment between molecular redox levels and metal Fermi levels play a crucial role in a large variety of observed electron transfer (ET) and transport phenomena. For example, the ability of redox molecules to be reversibly oxidized and reduced, in conjunction with the mentioned level alignment, allows for electrochemical gate control of the conductance through single redox molecules, in analogy with the mechanism operating in field effect transistors [6]. Noticeably, technological advance has allowed to track clearly the connection between improvement in junction conductance and metal-molecule level match [9]. As another example, the localization of the transferring charge around the molecular redox center and its stabilization by suitable polarization of the surrounding environment can account for observed behaviors of nonlinear charge transport, such as negative differential resistance (NDR) and hysteresis, that we have recently analyzed [10,11].

Redox molecular conduction junctions are junctions in which the molecular bridge connecting the metal electrodes can operate in more than one redox state. Such behavior requires that at least two conduction channels coexist: a fast channel that carries most of the observed current and a slow channel whose occupation determines the junction redox state and influences the conduction through the first channel. These junctions are often characterized by irreversible behavior, *i.e.*, at common voltage sweep rates the current response may be decoupled from the voltage change (hence, the current does not follow adiabatically the voltage), thus leading to memory effects (thermodynamic irreversibility) that appear as hysteresis over bias cycles. A similar mechanism underlies irreversibility in cyclic voltammetry of redox molecules under diffusionless [12] conditions. However, studies in the areas of voltammetry and molecular conduction junctions have mostly progressed separately so far. Connections between these two fields of study were proposed in a recent work [11] using a simple two-state molecular model (which corresponds to the slow charge-

* Corresponding author at: Department of Chemistry, Duke University, Durham, NC 27708, USA. Tel.: +1 919 6601633.
E-mail addresses: agostino.migliore@duke.edu (A. Migliore), nitzan@post.tau.ac.il (A. Nitzan).

http://dx.doi.org/10.1016/j.electacta.2015.01.174
0013-4686/

transport channel in the case of a junction). The analysis in Ref. [11] led us to an apparent contradiction: In cyclic voltammetry the threshold voltage scan rate for the onset of irreversible behavior is lower for larger reorganization energy of the redox molecular bridge. Therefore, given two systems with reorganization energies λ_1 and λ_2, and $\lambda_2 > \lambda_1$, the metal-molecule interface with reorganization energy λ_1 will behave ideally at voltage sweep rates for which the other interface shows already a distorted voltammogram. In general terms, the distortion of the voltammogram at a given scan rate increases with the reorganization energy. In contrast, the irreversibility in the response of a redox junction to a bias cycle, as measured by the maximum width of the hysteresis loop, appears to decrease with increasing reorganization energy of the (solvated) redox molecular bridge. Resolving this apparent contradiction is crucial to the understanding of the common mechanism for irreversibility within the two contexts. The solution of this issue is presented in this work (Section 4), after relating the mechanisms of charge transport through single and double metal-molecule interfaces (see Section 2) and after further investigating (compared to Ref. [11]) the onset of irreversibility in the charge flow through a single metal-molecule interface (Section 3). The reorganization energy of the redox molecular system generally plays a crucial role in determining the conditions for the onset of irreversibility, and the analysis of Section 3 leads to a procedure for estimating the reorganization energy from scan data of irreversible voltammetry.

2. Comparing the charge flow through single and double interfaces.

The Gurney [13]-Marcus [14,15]-Hush [16] theory of heterogeneous ET has been widely used both in the study of electrochemical reactions [17,18] at a metal electrode (where kinetic models based on Marcus charge transfer rates have been used in place of the traditional Butler–Volmer equations [1,18–21]) and in the context of "underwater" redox molecular junctions [10,22,23]. In both contexts, the solvation/reorganization energy of the redox molecular system plays a key role in determining the interfacial ET rate as well as in assisting charge localization and electrochemical gating [24,25]. In addition to the reorganization energy, the ET rate also depends on the electrode-molecule electronic coupling and on the minimum energy that is needed (at a given nuclear configuration) for electron transfer between the molecule and the metal, *i.e.*, the energy offset between the metal Fermi level and the effective molecular energy level (the latter is a measure of the energy difference between the two charging states of the redox molecular system [26]).

In Figs. 1a–e, we compare current measurements in molecular junctions and in voltammetric setups with strong molecular adsorption on the electrode, disregarding possible effects of diffusion, adsorption and desorption kinetics [27]. Fig. 1a depicts a three-electrode voltammetric configuration. The working electrode is coated with a layer of redox molecules. Under the assumed strong-adsorption conditions, the current across the surface of the working electrode is produced by charging or discharging the adsorbed molecular layer. Continuity is assured by inter-phase transport via transfer of some charged component to the solution phase [28,29]. This concomitant mechanism is here assumed to be efficient enough that the Marcus-type ET rate processes at the metal-molecule interface determine unambiguously the measured current.

In the setup of Fig. 1a, the voltage between the working and counter electrodes is kept constant, and the current between them is measured as a function of the potential difference between the working and reference electrodes. This so-called overpotential changes the alignment between the molecular electron level and the Fermi energy, and is therefore equivalent to a gate potential in transistor physics. The ideal behavior of the current–voltage response under reversible conditions (that is, when the potential scan rate is low enough for the concentrations of oxidized and reduced molecules to satisfy the Nernst equation) shows no separation between the anodic and cathodic peaks (Fig. 1b). Then,

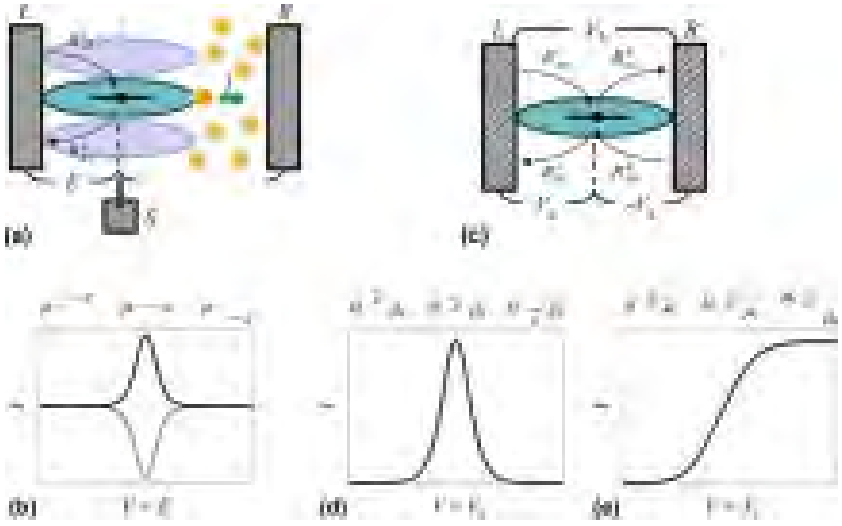

Fig. 1. (*a*) Voltammetric three-electrode configuration. The working electrode (*L*) is coated with a monolayer of strongly adsorbed redox molecules. A molecule is highlighted in cyan (its contact with the metal can be compared with the semi-junction in panels *c*). An overpotential *E* is applied between *L* and a reference electrode *S*. The charge flow due to ET at the metal-molecule interface is continued by electrolyte (depicted as yellow circles) in solution to the counter electrode *R* (this current *I* is measured). (b) Ideal voltammogram with equal anodic and cathodic peaks, for slow enough overpotential scan rate and after subtracting the baseline [1]. The relative alignment of the electrode chemical potential μ (yellow dash) and the overvoltage-dependent molecular energy level (cyan dash) $\varepsilon(E) = E_B - E_A - eE$ is shown at different values of the overpotential. The peak in the current occurs when $\varepsilon = \mu$ (see Eqs. (4b) and (7)). (c) Schematic view of a metal-molecule-metal redox junction, where the molecular level may be shifted by the gate voltage V_g relative to the left (*L*) and right (*R*) metal Fermi levels or the electrode Fermi levels may be shifted with respect to each other by a bias voltage V_b. The rate constants for the interface ET processes are described in the main text. (d) A peak in the I–V_g response of the junction in panel *c* corresponds to the passage of the molecular level across the Fermi window, at a fixed bias voltage $\overline{V}_b = (\mu_L - \mu_R)/e$ between the electrodes. *I* is measured between the *L* and *R* electrodes. (e) *I* vs. V_b. The high-V_b plateau is attained once the molecular level is sufficiently inside the Fermi window, which grows with V_b. (For interpretation of the references to colour in this figure legend, the reader is referred to the web version of this article.)

for the case of one-electron transfer between the lead and the redox species, the peak potential is simply the reduction potential of the redox couple [1,11]. The current falls off as the redox layer is fully reduced or oxidized. Denoting by P the probability that a molecule is in a given oxidation state, dP/dt is the (dimensionless) charge flow at the interface on a per molecule basis. Changing the overpotential E [30], this current reaches a maximum at the E value for which P has an inflection point, and vanishes when P approaches unity or zero. In contrast, in a junction P is a steady-state property and dP/dt is the rate of total charge exchange between the molecular bridge and both electrodes (see Section 4). In fact, the inter-phase transport that intervenes in the voltammetric context marks a significant difference with the redox junction context, although the current across the working electrode surface shares important features with that across each electrode-molecule interface in a junction (in particular, the mechanism underlying irreversibility that is discussed in Sections 3 and 4).

In the case of Fig. 1a–b, the adsorbed redox molecule is charged at high enough interfacial voltage, an equivalent charge moves in the adjacent bulk phase to the counter electrode (*e.g.*, when quinones are the adsorbed redox species, changes in their oxidation states are accompanied by simultaneous hydrogen ion transfer to the bulk electrolyte phase [28,31]), and afterwards that redox molecule no longer contributes to the current, unless it can be reversibly discharged in the downward potential scan and thus contributes to the negative current peak in Fig. 1b. In a junction, changing the gate voltage V_g as shown in Fig. 1c, the molecular level is moved relative to the left and right electrodes (between which the current is measured) similarly to Fig. 1b, and one obtains the I–V curve of Fig. 1d. However, the same molecule can be repeatedly charged by the left electrode and discharged by the right one at gate voltages such that the molecular level is inside the electrodes Fermi window at a fixed bias voltage (with clear implications on the evolution and maximum value of the occupation probability P as a function of the gate voltage). The current vanishes as the molecular level exits the Fermi window at sufficiently small or large gate voltages. A different behavior is seen when the bias voltage, V_b, is changed in a junction, as shown in Fig. 1c, thus producing I–V responses such as in Fig. 1e. The resulting potential difference across a given (*e.g.*, the left) electrode-molecule interface shifts the molecular level with respect to the electrode Fermi level, similarly to what occurs in the other two cases. However, the shift with respect to the other Fermi level is in the opposite direction compared to the case of Fig. 1d. In fact, the molecular level enters and remains inside the Fermi window, as the latter grows with the applied bias voltage, and the current correspondingly levels off at its high-voltage value in the represented two-state model [11].

The description of the I–V response in terms of a molecular level is complicated by the presence of the reorganization energy in the hopping model of Fig. 1c. In this model, A and B denote the oxidized and reduced states of the (solvated) redox molecule and have equilibrium energies E_A and E_B, respectively; R^L_{AB} is the rate constant for the forward electron injection from the L electrode that reduces the molecule ($A \to B$); R^R_{BA} is the rate of the electron delivery to the R metal that oxidizes the molecule ($B \to A$); R^L_{BA} and R^R_{AB} are the backward ET rate constants, which rapidly decrease for increasing $V_b > 0$. When V_g is increased, the energy of the electron localized on the bridge goes down by $-eV_g$. The injection rate R^L_{AB} becomes significant for [10] $V_g \gtrsim (\lambda + E_{AB} - \mu_L)/e$, namely, when $E_{AB} - eV_g \lesssim \mu_L - \lambda$, with $E_{AB} \equiv E_B - E_A$. $-V_g$ is the potential difference between the molecular redox center and the R electrode. Therefore, R^R_{BA} decreases with V_g and is appreciable [10] for $-V_g \gtrsim (\lambda - E_{AB} + \mu_R)/e$, that is, as long as $\mu_R + \lambda \lesssim E_{AB} - eV_g$. The current through the junction modeled in Fig. 1c is appreciable only if both R^L_{AB} and R^R_{BA} are such. Hence, the molecular reorganization energy λ, the redox state energy difference E_{AB}, and the fixed bias voltage $\overline{V}_b = (\mu_L - \mu_R)/e$ need to satisfy the double condition $\mu_R + \lambda \lesssim \varepsilon(V_g) \equiv E_{AB} - eV_g \lesssim \mu_L - \lambda$ over a finite range of V_g in order to attain a maximal peak current in a V_g sweep. For sufficiently small λ, the optimal value of V_g for electron conduction through the redox molecule is given by the relationship $\varepsilon(V_g) \approx (\mu_L + \mu_R)/2$. For zero λ and negligible inner-shell electronic relaxation in the molecule after its charging, $\varepsilon(V_g)$ is the V_g-dependent molecular electronic level, and the maximum current through the junction is achieved when the molecular single-electron energy is exactly at the middle of the electrode Fermi window.

When the bias voltage is changed, the forward ET rate with larger threshold (interfacial) voltage for its increase determines the bias needed for the current rise to its high-voltage value. For $E_{AB} > \mu_L$, R^L_{AB} is the limiting ET rate and the current significantly increases when $\varepsilon(V_b) \equiv E_{AB} - eV_b/2 \gtrsim \mu - \lambda$, where μ is the unbiased chemical potential of the L metal. For negligible λ and inner-shell electronic relaxation, this condition describes the crossing of μ and the molecular energy level.

Despite the differences among the three situations described above, the underlying mechanism for the onset of irreversible behavior in the current–voltage response is similar. Charge localization on the redox molecular system slows down the heterogeneous ET rates so that the ET time scale becomes comparable to the measurement time scale under changing external conditions. Irreversibility in the system response reflects its inability to instantaneously adjust to the changing external conditions, and was investigated in Ref. [11] for both the voltammetric and redox junction systems. The detailed behavior is however different in the single electrode case and in the junction, as discussed in the next sections using a simple two-state redox system.

3. Sweep rate-dependent effect of the molecular reorganization energy on the cyclic voltammograms of diffusionless redox adsorbates.

The discussion in the introduction and Ref. [11] has pointed out the importance of the coexistence of at least two transport channels for the realization of significant redox behavior in molecular junctions. However, the analysis of the conditions for irreversible behavior is most easily performed by using a simple two-state model of the molecular system for both the single and double metal-molecule interface systems. In fact, these two states correspond to the slow transport channel in the multi-state models of Ref. [11], and this channel is responsible for the switching of the other faster channel between two different conduction modes and for the occurrence of hysteresis in weakly coupled redox junctions. Thus, we use a two-state model to describe both single (Fig. 1a) and double (Fig. 1c) metal-molecule interfaces. For the transitions between these states we adopt a classical rate picture (diagonal density matrix) with nuclear reorganization occurring in a time scale much faster than the average time between different ET steps. Therefore, the electronic dynamics consists of ET processes that connect different charging states of the molecule at the respective equilibrium nuclear coordinates. The single metal-molecule interface is studied in this section

We denote by P_A and P_B the probabilities that the active adsorbed (and solvated) molecule is in the A and B oxidation states, respectively. The corresponding equilibrium values are denoted $P_{A,\mathrm{eq}}$ and P_{eq}. Since $P_A + P_B = 1$, we often use a single variable $P = P_B = 1 - P_A$ to describe these variables. The rate constants for

electron injection ($A \to B$) and removal ($B \to A$) are denoted $R_{AB} \equiv R_{A\to B}$ and $R_{BA} \equiv R_{B\to A}$, respectively. These rates are related to the equilibrium probabilities by the detailed balance condition $P_{A,\mathrm{eq}}R_{AB} = P_{\mathrm{eq}}R_{BA}$. Clearly, $P_A + P_B = P_{A,\mathrm{eq}} + P_{\mathrm{eq}} = 1$. These rates are obtained [10] from the Marcus theory for heterogeneous ET [14,15] in the forms

$$R_{AB} = \frac{\gamma}{4}S(\lambda,T,\alpha)\exp\left[-\frac{(\alpha-\lambda)^2}{4\lambda k_B T}\right],$$

$$R_{BA} = \frac{\gamma}{4}S(\lambda,T,\alpha)\exp\left[-\frac{(\alpha+\lambda)^2}{4\lambda k_B T}\right]$$

with

$$\alpha \equiv \mu - E_{AB} + eV, \tag{1b}$$

$$S(\lambda,T,\alpha) = \sum_{n=0}^{N}\frac{1}{2^n}\sum_{j=0}^{n}(-1)^j\binom{n}{j}\left[\eta_j(\lambda,T,\alpha)+\eta_j(\lambda,T,-\alpha)\right], \tag{1c}$$

$$\eta_j(\lambda,T,\alpha) = \exp\left\{\frac{[(2j+1)\lambda+\alpha]^2}{4\lambda k_B T}\right\}\mathrm{erfc}\left[\frac{(2j+1)\lambda+\alpha}{2\sqrt{\lambda k_B T}}\right], \tag{1d}$$

where V is the overpotential [30,32], N truncates the otherwise infinite sums, γ is the coupling strength to the electrode and is here assumed to be a constant, k_B is the Boltzamann constant, T is the temperature, μ is the chemical potential of the electrode (for $V = 0$), λ is the reorganization energy of the molecular system, and $E_{AB} \equiv E_B - E_A$, where E_A and E_B are the energies of states A and B, respectively. Since the transferring electron charge localizes at the redox site, the ET between the molecule and the electrode (or each of the two electrodes in a junction) is described by assigning effective (average) electrostatic potentials to the corresponding regions [10]. However, the main conclusions of our study do not depend on the detailed spatial distribution of the voltage across the molecule (either in the single molecule-electrode interface or in the junctions of Section 4). The overpotential V is assigned as positive when the electrostatic potential on the molecule is higher than that in the metal [10], which amounts to the negative of the traditional definition of overpotential. These rates, within a simple kinetic scheme [11,19,27], yield the current expression [11]

$$J \equiv \frac{I}{e} = \frac{dP(V(t),t)}{dt} = (1-P)R_{AB}(V) - PR_{BA}(V) = -\rho Q \tag{2}$$

where e is the magnitude of the electron charge, ρ is the effective relaxation rate, given by

$$\rho = R_{AB} + R_{BA} \tag{3}$$

and Q is the departure of P from P_{eq}, given by

$$Q(V,t) = P(V,t) - P_{\mathrm{eq}}(V) = P_{A,\mathrm{eq}}(V) - P_A(V,t) \tag{4a}$$

with

$$P_{\mathrm{eq}}(V) = \frac{R_{AB}(V)}{R_{AB}(V)+R_{BA}(V)} = \frac{1}{1+\exp\left(\frac{E_{AB}-\mu-eV}{k_B T}\right)} \tag{4b}$$

Q depends explicitly on the time t and incorporates all the memory effects in the response of the system to the external voltage V. In Ref. [11], we showed that under reversible conditions (that is, when the voltage change is much slower than any other process in the system) Eq. (2) becomes

$$J = u\frac{dP_{\mathrm{eq}}}{dV} = -\rho(P - P_{\mathrm{eq}}) \tag{5}$$

where $u = dV/dt$ is the rate of the voltage sweep (Q vanishes with u). In this slow u limit, the charging state of the adsorbed redox molecular layer adapts quasi-statically to the changing voltage. That is, a very small (virtually infinitesimal) deviation $Q = P - P_{\mathrm{eq}}$ is produced by the voltage change dV and, at any V, the interfacial electron transitions, with an overall rate $\rho(V)$, are able to restore the equilibrium value of P at $V + dV$, $P_{\mathrm{eq}}(V + dV)$. Thus, the departure Q of P from $P_{\mathrm{eq}}(V)$ remains infinitesimal during a voltage scan, namely, there is no appreciable accumulation of the spurious, time-dependent component $Q(V,t)$ of P. In fact, in Ref. [11], the range of sweep rates that lead to this reversible behavior was derived from

$$\frac{|Q|}{P_{\mathrm{eq}}} \equiv \frac{|P - P_{\mathrm{eq}}|}{P_{\mathrm{eq}}} = \frac{u}{\rho P_{\mathrm{eq}}}\frac{dP_{\mathrm{eq}}}{dV} = \frac{dP_{\mathrm{eq}}/dt}{R_{AB}} << 1 \tag{6}$$

(at any voltage that produces appreciable current). Conversely, the failure of this condition was used to formulate a threshold V-scan rate for the first appearance of irreversibility over a voltage sweep or cycle. The last ratio in Eq. (6) was absent in Eq. (7) of Ref. [11] and is derived from Eqs. (3) and (4b). This ratio compares directly the interfacial ET rate, R_{AB}, and the rate of change in molecular occupation, dP_{eq}/dt, that needs to be sustained for reversibility.

Since $dP_{\mathrm{eq}}/dt = udP_{\mathrm{eq}}/dV$, the most stringent test for the validity of Eq. (6) is around the voltage

$$V_0 = (E_{AB} - \mu)/e \tag{7}$$

that corresponds to crossover of the forward and backward ET rates ($R_{AB} = R_{BA}$) and hence to maximum dP_{eq}/dV, namely, to the maximum per-molecule current edP_{eq}/dt across the interface under reversible conditions. So, if Eq. (6) is satisfied around $V = V_0$, a reversible current-voltage response is expected over the whole overvoltage scan. At $V = V_0$, Eq. (6) implies that the voltage change over the characteristic time (for the interfacial ET dynamics) $1/\rho$, $\delta V = u/\rho$, is negligible compared to the thermal voltage $k_B T/e$. More precisely,

$$\delta V\frac{dP_{\mathrm{eq}}}{dV}\Big|_{V_g=V_0} = \frac{e}{4k_B T}\delta V << P_{\mathrm{eq}}(V_0) = \frac{1}{2} \Rightarrow \delta V \equiv \frac{u}{\rho} << \frac{2k_B T}{e} \tag{8}$$

which is a consequence of the thermal equilibrium inherent in Eq. (4b). Eq. (8) imposes the following upper bound for the reversible scan rate [11]:

$$u << u_l(V_0;\gamma,\lambda,T) \equiv 2\frac{k_B T}{e}\rho(V_0;\gamma,\lambda,T) \tag{9a}$$

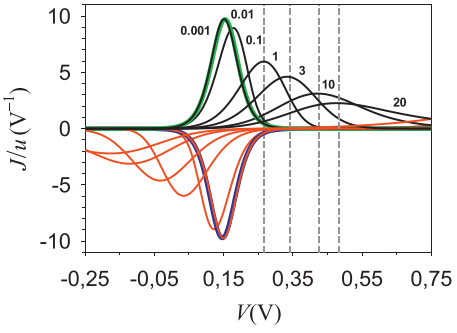

Fig. 2. J/u plotted against V, using Eqs. (1–2) with model parameters: $T = 298$ K, $E_{AB}-\mu = 0.15$ eV, $\lambda = 0.25$ eV, $\gamma = 10^2\,\mathrm{s}^{-1}$ and the overpotential scan rates in V/s indicated near the voltammograms. The upward and downward voltage sweeps are represented in black and red, respectively, except for the case in which the sweep rate is $u = 0.01$ V/s (green and blue) to distinguish from the case $u = 0.001$ V/s. The vertical dashes locate the peak potentials predicted by Eq. (13). The same diagram is obtained by scaling γ and u by the same factor (*e.g.*, for $\gamma = 10^6\,\mathrm{s}^{-1}$, the largest scan rate is 2×10^5 V/s, which would amount to ultrafast cyclic voltammetry [35]). (For interpretation of the references to colour in this figure legend, the reader is referred to the web version of this article.)

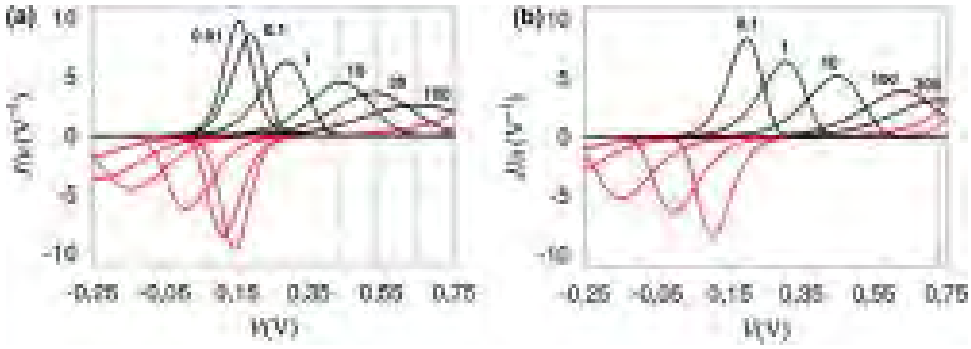

Fig. 3. J/u versus V from Eqs. (1–2), with the indicated sweep rates, in V/s, and the model parameters: $T = 298$ K, $E_{AB} - \mu = 0.15$ eV, and (a) $\lambda = 0.5$ eV, $\gamma = 10^3\ s^{-1}$, (b) $\lambda = 0.75$ eV, $\gamma = 10^4\ s^{-1}$. Color code as in Fig. 2. The vertical dashed lines locate the peak potentials predicted by Eq. (13). $u_l \cong 0.15$ V/s and $u_l \cong 0.12$ V/s in panels a and b, respectively (u_l decreases with λ despite the increase in γ).

with

$$\rho(V_0;\gamma,\lambda,T) = \begin{cases} \gamma & (\lambda = 0) \\ \gamma\sqrt{\dfrac{\pi k_B T}{\lambda}}\exp\left(-\dfrac{\lambda}{4k_B T}\right) & (\lambda >> k_B T) \end{cases} \quad (9b)$$

Conversely, for $u \gtrsim u_l$, P cannot adapt to the changing overvoltage so as to satisfy Eq. (6). The consequent delay in the evolution of P over a voltage cycle leads to a peak potential $V_{peak}^{up} > V_0$ in the upward sweep and $V_{peak}^{down} < V_0$ in the downward sweep. The peak potential separation under irreversible conditions has been widely studied [1], but the focus has not been on the hysteresis in P, which is indeed a source of both the distortion from ideal (reversible) voltammogram shape and the hysteretic current–voltage response in molecular conduction junctions.

Typical voltammograms calculated from Eq. (2), using the finite-difference procedure described in Ref. [19] with ET rate constants expressed as in Eq. (1), are shown in Figs. 2 and 3. The observed behavior can be interpreted using Eq. (9). The physical parameters used in Fig. 2 give $u_l \approx 0.2$ V/s. This threshold value agrees with the ideal peaks obtained for $u = 0.01$ V/s and the onset of peak distortion for u comparable to u_l (in particular, see voltammogram for $u = 0.1$ V/s). Note that current-overpotential responses of the type shown in Figs. 2 and 3 are observed experimentally [33,34]. Furthermore, as predicted by our theoretical analysis for a wide range of chemical–physical parameters, the deviation of cyclic voltammograms from the ideal shape is appreciable for overvoltage scan rates on the order of 0.1 V/s or larger.

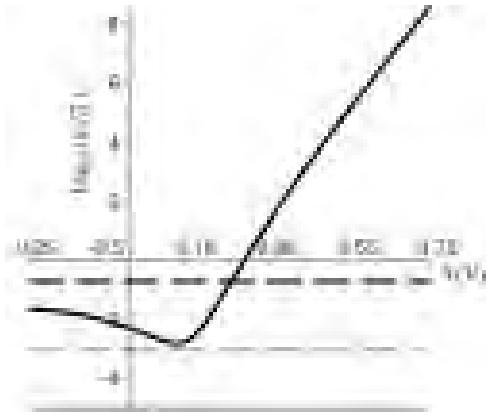

Fig. 4. $\log_{10}(u_l/\bar{u})$, with $\bar{u}/\gamma = 1$V, versus V, according to Eq. (10). The interface was modeled using the same parameters as in Fig. 2. The quantity $\log_{10}(u/\bar{u})$ is also represented, for $u = 0.001$ V/s (grey solid line), 0.01 V/s (grey dash) and 20 V/s (black dash).

The reversible behavior for $u << u_l$ is characterized by Eqs. (4b) and (7), and thus does not depend on the reorganization energy λ, while the irreversible behavior and its first appearance near $V = V_0$ for $u \gtrsim u_l$ strongly depend on λ, as shown by comparing Figs. 2 and 3a–b. This dependence is also related to the voltage range in which the system is operating. Thus, it may be relevant to establish a limiting scan rate u_l (which separates the u regimes of reversible and irreversible current–voltage response) at each V [11]:

$$u_l = \frac{\rho P_{eq}}{dP_{eq}/dV} = 2\frac{k_B T}{e}\tilde{\rho}(V;\gamma,\lambda,T) \quad (10a)$$

where

$$\tilde{\rho}(V;\gamma,\lambda,T) = \frac{e}{2k_B T}\frac{P_{eq}}{dP_{eq}/dV}\rho(V;\gamma,\lambda,T)$$
$$= \begin{cases} \gamma & (\lambda = 0) \\ \gamma\dfrac{S(\lambda,T,\alpha)}{8}\left[1+\exp\left(-\dfrac{\alpha}{k_B T}\right)\right]^2 \\ \times\exp\left[-\dfrac{\left(\lambda-\alpha+2\sqrt{\alpha\lambda}\right)\left(\lambda-\alpha-2\sqrt{\alpha\lambda}\right)}{4\lambda k_B T}\right] & (\lambda \neq 0) \end{cases} \quad (10b)$$

From the comparison of Eqs. (9a) and (10a) $\tilde{\rho}$ is seen as an effective relaxation rate of the molecular system that characterizes its response to changing overvoltage. $\tilde{\rho}$ takes into account the actual ET rates through ρ and the rate of the relative change in P_{eq} through $d\ln P_{eq}/dV$. The smaller the sensitivity of P to the changing V (around a given value), the larger the effective relaxation rate (or, in other words, the smaller the actual ET rates needed to assure reversibility). For example, for large enough V, the molecular redox site is permanently occupied by the transferring charge ($P_{eq} = 1$), hence $\tilde{\rho} \to \infty$.

The limiting sweep rate in Eq. (10) is plotted against the overvoltage V in Fig. 4, where it is compared with three of the sweep rate values used in Fig. 2, for a system characterized by the same parameters. $u = 0.001$ V/s is much smaller than u_l, thus yielding a reversible peak in Fig. 2. $u = 0.1$ V/s is close enough to u_l to produce hysteresis over the V range spanned by the reversible peak. Only the tail of the current peak appears in this range for $u = 20$ V/s (cf. peaks for $u = 0.001$ V/s and $u = 20$ V/s in Fig. 2), because of the significantly delayed evolution of P compared to that of P_{eq} for $u >> u_l$.

The shapes of voltammograms such as those in Figs. 2 and 3, and their dependence on the scan rate, have been studied by using both the Butler–Volmer equations and the Marcus theory of

interfacial ET [1,18–21,27,36–38]. In Ref. [37] experimental cyclic voltammograms were modeled reasonably well in terms of the Marcus theory and, to a lesser extent, in terms of the empirical Butler–Volmer model. Conversely, Ref. [38] observes a better performance of the Butler–Volmer approach, compared to the Marcus model, to describe cyclic voltammetry in solution-phase systems whose transfer coefficients [17] deviate significantly from $^1/_2$. However, the Butler–Volmer equations are empirical and are given theoretical justification for a transfer coefficient of $^1/_2$ because of the exponential behavior of the Marcus ET rates at low values of the overpotential [1]. Whatever the model used, the analysis of the peak position as a function of the voltage is less sensitive to the choice of the baseline than the peak shape analysis, and thus is preferred to the latter to determine the standard rate constant [1], namely, the common value of the two ET rate constants at zero driving force, for which the reorganization energy λ is the only free energy parameter involved in the Marcus formulation.

The great mechanistic importance of the reorganization energy has motivated several strategies for the estimation of its value from cyclic voltammograms [1]. Indeed, λ measures the ability of the solvated molecular system to stabilize the transferring excess charge at the redox center, thus making the interfacial ET rates (and hence the effective relaxation rate in Eq. (10b)) small enough for the appearance of significant irreversibility at common sweep rates. Therefore, while the above analysis focused on the λ-dependence of the threshold sweep rate for the occurrence of irreversibility, the remaining part of this section is dedicated to the relationship between the appearance of the irreversibility (as described and measured by the shift in peak potential) and λ, which also results in a procedure to evaluate λ.

The analysis of the interfacial ET dynamics needed to relate λ to the peak potential V_{peak} is simplified over V ranges where one of the two interfacial ET rates is negligible, so that the ET event is irreversible. In particular, Fig. 5 and its comparison with Fig. 2 show that, for large enough u, the peak in the current takes place at voltages well above V_0, where $R_{AB} >> R_{BA}$ and the molecule-to-metal ET process is suppressed. In this limit of irreversible electrode reaction [39], when the voltage scan rate is such that $P(V)$ substantially fails to follow $P_{eq}(V)$ (which remains close to unity), $dP/dt \cong dQ/dt$ and Eq. (2) gives approximately

$$\frac{dQ}{dt} = -R_{AB}Q \tag{11}$$

Using the Hale approximation [17,40] to R_{AB}, taking the time derivative of Eq. (11) and considering that at the peak voltage V_{peak} it is $d^2P_{eq}/dt^2 \cong d^2Q/dt^2 = 0$, one obtains

$$\mathrm{erfc}^2(x) = \frac{2eu}{\gamma\sqrt{\pi\lambda k_B T}}\exp(-x^2) \tag{12a}$$

where

$$x \equiv \frac{\lambda + E_{AB} - \mu - eV_{peak}}{2\sqrt{\lambda k_B T}} \tag{12b}.$$

Eq. (12) was similarly derived in Ref. [19] from the rate equation for the mole fraction of oxidized adsorbate. However, although the critical role of the peak positions in determining free energy parameters such as redox potentials and reorganization energies, the analytical solution of Eq. (12) is missing in the literature. Here, we extend the treatment of Ref. [19] by providing an analytical solution for the peak potential as a function of λ, γ, and u. The resulting expression for the peak potential is (see Appendix A):

$$V_{peak} = \frac{\lambda + E_{AB} - \mu}{e} - \frac{2\sqrt{\lambda k_B T}}{e}\left(\sqrt[3]{-\frac{\nu}{2} + \sqrt{\frac{\nu^2}{4} + \frac{\eta^3}{27}}} + \sqrt[3]{-\frac{\nu}{2} - \sqrt{\frac{\nu^2}{4} + \frac{\eta^3}{27}}} - \frac{A}{3}\right) \tag{13a}$$

with

$$\begin{cases} \eta = -\frac{1}{3}A^2 + B \\ \nu = \frac{2}{27}A^3 - \frac{1}{3}AB + C \end{cases} \tag{13b}$$

where

$$\begin{cases} A = \dfrac{1+6p^2}{p(3+2p^2)} - \dfrac{a_1 p}{3+2p^2}\dfrac{1}{D} \\ B = \dfrac{6}{3+2p^2} - \dfrac{2a_1 + a_2}{3+2p^2}\dfrac{1}{D} \\ C = \dfrac{2}{p(3+2p^2)} - \dfrac{1}{p(3+2p^2)}\dfrac{1}{D} \end{cases} \quad \text{for } 0 \le x < 1 \quad \Rightarrow \quad \frac{\lambda + E_{AB} - \mu}{e} - \frac{2\sqrt{\lambda k_B T}}{e} < \mathrm{V} \le \frac{\lambda + E_{AB} - \mu}{e} \tag{13c}$$

or

$$\begin{cases} A = \dfrac{(1+6p^2)D + (a_1 - 6)p^2 - 2}{p[-(3+2p^2)D + 2(3+p^2)]} \\ B = \dfrac{6 - 6D - 2a_1 - a_2}{-(3+2p^2)D + 2(3+p^2)} \\ C = \dfrac{2D - 1}{p[-(3+2p^2)D + 2(3+p^2)]} \end{cases} \text{for } -1 < x \le 0 \Rightarrow \frac{\lambda + E_{AB} - \mu}{e} < \mathrm{V} \le \frac{\lambda + E_{AB} - \mu}{e} + \frac{2\sqrt{\lambda k_B T}}{e} \tag{13d}$$

with the dimensionless constant

$$D = \left[\frac{e^2u^2}{4\pi\lambda k_B T\gamma^2}\right]^{\frac{1}{4}} \tag{13e}$$

and $a_1 = 0.3480242$, $a_2 = -0.0958798$, $a_3 = 0.7478556$ (notice that $a_1 + a_2 + a_3 = 1$) and $p = 0.47047$. Eq. (13) is valid in the thermodynamically irreversible limit of Eq. (11) and under the condition $D \lesssim 1$, which holds, *e.g.*, for all cases represented in the above figures. Eq. (13) gives a good approximation to the peak potential over a significant V range (compared to the overpotential ranges generally spanned in cyclic voltammetry) that encompasses the threshold voltage [10] $(\lambda + E_{AB} - \mu)/e$ for the rise of R_{AB}. The voltage range in which the approximation is valid increases with λ and T.

The dashed lines in Figs. 2 and 3 mark peak potentials obtained by using Eq. (13). The midpoint of the V range of applicability of Eq. (13) is out of the spanned overpotential range in Fig. 3b, but Eq. (13) can be still applied to current peaks of appreciable

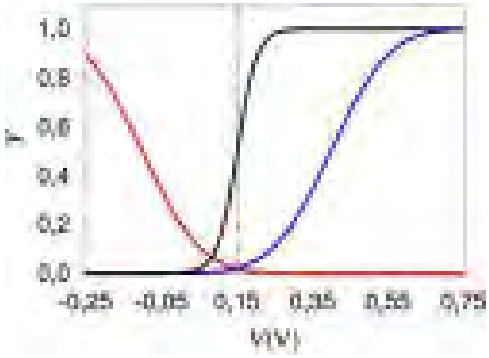

Fig 5. $Y = R_{BA}/\gamma$ (red), R_{AB}/γ (blue) and P_{eq} (black) plotted against V, modeling the interface with the same physical parameters as in Fig. 2. The dashed line marks the overvoltage V_0, where $R_{AB} = R_{BA}$. (For interpretation of the references to colour in this figure legend, the reader is referred to the web version of this article.)

magnitude. Moreover, the analytical derivation of Eq. (13) given in the Appendix A ensures its validity, within the Marcus [14,15]–Chidsey [18] model, also over overvoltage ranges where the localization of the flat current peaks is otherwise difficult, or unfeasible, and yet of theoretical interest, for example for the estimation of reorganization energy [1,19,41].

It is worth noting that Eq. (12) also yields the asymptotic behavior of V_{peak} for very large scan rates in the form (see Appendix A)

$$V_{peak} \cong \frac{\lambda + E_{AB} - \mu}{e} + \frac{2}{e}\sqrt{\lambda k_B T \ln\left(\frac{e}{2\gamma\sqrt{\pi\lambda k_B T}}u\right)} \tag{14}$$

This asymptotic behavior differs from the constant value for the peak potential as a function of the scan rate u that is guessed in Ref. [19] (within the same Marcus–Chidsey framework) based on the trend in Fig. 2 therein. Eq. (14) also differs from the logarithmic dependence of the peak potential on u that was obtained by Laviron [27] using Butler–Volmer equations. Since a Taylor expansion of Eq. (14) over a relatively small u range yields a linear dependence of V_{peak} on $\ln(u)$, the relative applicability of Eq. (14) and Laviron's method can be judged by fitting experimental data over sufficiently large scan rate ranges. For example, it would be desirable to investigate the applicability of Eq. (14) to the cyclic voltammograms on cytochrome c and hemin-doped human serum albumin in Ref. [34], where Laviron's theory was used to extract protein-metal ET rate constants from voltammetric measurements over relatively small u ranges.

A strategy to evaluate λ is suggested directly by Eq. (12) or (13), noting that for $x = 0$, namely, for

$$V_{peak} = \frac{e}{\pi k_B T}\left(\frac{2u}{\gamma}\right)^2 + \frac{E_{AB} - \mu}{e} \tag{15}$$

Eq. (12a) or Eq. (13) yields

$$\lambda = \frac{1}{\pi k_B T}\left(\frac{2eu}{\gamma}\right)^2 \tag{16}$$

In fact, when the Marcus–Chidsey model can be employed, one can obtain λ by means of the following procedure: (i) the energy gap $E_{AB} - \mu$ is determined from the value of the peak potential at low enough sweep rate (*i.e.*, in reversible conditions); (ii) sweeps at different u values are performed and, once V_{peak} has the value resulting from Eq. (15), the reorganization energy is given by Eq. (16). However, a direct use of Eqs. (15) and (16) to obtain the reorganization energy requires a previous separate estimate of the electrode-molecule coupling strength γ, which is the high-V plateau of R_{AB} (see Fig. 5). Proceeding in this way one may incur the complication that the interfacial ET rate is limited by a process that is distinct from ET, so that the leveling off of the resulting apparent ET rate is wrongly interpreted as the achievement of the high-V plateau of R_{AB} and λ is overestimated, which is a common problem in the interpretation and use of voltammetric data to determine the reorganization energy [1,19,37,41]. As an alternative, one may use two measured V_{peak} values and the corresponding u values to obtain γ and λ from Eq. (12) or more simply from Eq. (13). Note that γ is also related to the plateau current that is approached for sufficiently high bias in a metal-solvated redox molecule-metal junction where the same type of metal-molecule interface and molecular conduction channel are involved [11].

4. Reorganization energy effects on the hysteretic response of a redox junction.

In this section we clarify an apparent contradiction that was raised in Ref. [11] and plays an important role in relating the current–voltage responses of voltammetry and junction setups that use redox molecules: When two molecular redox states are involved in the conduction, the distortion of cyclic voltammograms at a given overpotential sweep rate is larger for larger reorganization energy of the adsorbed redox layer; instead, the maximum width of the hysteresis loop obtained from a fast bias cycle on a junction is larger for smaller reorganization energy of the redox molecular bridge. Understanding the physical reasons for these contrasting irreversible effects of the λ value in the two cases is important for connecting the different ideal or non-ideal behaviors observed in voltammetry and redox molecular junction experiments. Understanding how redox properties that are precisely measured via voltammetry are expressed in junction setups is important for the design of redox molecular junctions with desired memory properties.

In Section 3, the irreversibility in the response of the system to a changing external potential difference was introduced in the analysis by expressing the current in terms of the metal-molecule ET rates and the probability P of the redox system occupation by injected charge, and inspecting the departure of P from its equilibrium values while the overpotential is changed. This analysis led to a measure for overvoltage scan rates that may or may not produce irreversible I–V response. In this section, we use the same type of approach to investigate the connections between the redox probability P, the interfacial ET rates, and the current in a junction, emphasizing similarities and differences with the corresponding connections in a single metal-molecule interface of a voltammetric setup. Through this analysis, we explain the relation between λ value and hysteresis in metal-molecule-metal junctions.

The R^K_{AB} and R^K_{BA} rates are described by Eq. (1), except that α is replaced by $\alpha_K \equiv \mu - E_{AB} - e\phi_K$ (K=L, R), where ϕ_K denotes the potential of the K (= L, R) electrode relative to the molecule redox site. Without loss of generality for our conclusions, we assume symmetric molecule-electrode contacts, with coupling strength γ and symmetric potential drops across the two interfaces, so that $\phi_R = V/2 = -\phi_L$ [10]. The L- and R-terminal currents are

$$J_L \equiv I_L/e = (1-P)R^L_{AB} - PR^L_{BA} = J_{AB} - (R^L_{AB} + R^L_{BA})Q \tag{17}$$

and

$$J_R \equiv I_R/e = PR^R_{BA} - (1-P)R^R_{AB} = J_{AB} + (R^R_{AB} + R^R_{BA})Q \tag{18}$$

where the steady-state current

$$J_{AB} = \frac{R^L_{AB}R^R_{BA} - R^R_{AB}R^L_{BA}}{R_{AB} + R_{BA}} \tag{19}$$

is clearly the same through both interfaces. Away from steady-state, the L- and R-terminal currents are in general not equal and the net (average) charging on the molecular bridge is given by [42]

$$J_L - J_R = -(R_{AB} + R_{BA})Q = dP/dt \tag{20}$$

Here Q is still defined by Eq. (4a), but P_{eq} is replaced by P_{ss}, that is the (nonequilibrium) steady-state probability to find the molecular system in state B. With this replacement, the relationship between P_{ss} and Q during reversible voltage sweeps is again described by Eqs. (5) and (6). However, in the junction, both interfaces contribute to the redox transitions of the bridge: $R_{AB} = R^L_{AB} + R^R_{AB}$ and $R_{BA} = R^L_{BA} + R^R_{BA}$. This fact causes important differences between the charge transport across single and double metal-molecule interfaces.

A main difference lies in the connection between population of the redox system and current through the interface(s). In the voltammetric setup, the current through the surface of the coated electrode results from charging the adsorbed redox molecules (see Sections 2 and 3). Consequently, the current vanishes for large enough overvoltage, when $P = P_{eq} = 1$. In a junction, where the same redox system participates in ET with source and drain, the rate of charge accumulation in the molecular bridge, dP/dt, amounts to the difference in the L- and R-terminal currents. Thus, the relation between molecular charge and current under reversible conditions, which was provided by Eq. (5) for the single interface, is now described by the steady-state regime condition

$$-\rho Q = u\frac{dP_{ss}}{dV} = J_L - J_R \tag{21}$$

with exact steady-state achieved for $u = 0$, and hence $J_L = J_R$. Steady-state and reversibility conditions are equivalent in a two-state model. Indeed, the comparison of Eq. (20) with Eqs. (17) and (18) shows that the steady-state operation, which is defined by $|J_L - J_R|/J_{AB} \cong 0$, is a sufficient condition for reversibility, since it implies that the last terms in Eqs. (17) and (18) are negligible compared to the respective currents. In other words, under reversible conditions, the rate of charge storage in the redox system is seen as a peak in the current that decreases proportionally to the scan rate u in a voltammogram [36,43], while its effect on the conduction is disregarded in a junction.

The differences in the behaviors of P_{eq} (molecular average occupation in the single interface) and P_{ss} (in a double interface) during a potential sweep are noteworthy, and are reflected in the corresponding currents (see also Eq. (25)). For $V \geq 0$, R^R_{AB} is negligible and the connection between P_{ss} and P_{eq} can be written as

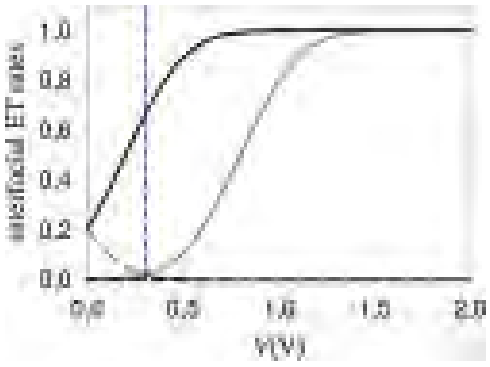

Fig. 6. Voltage dependence of the interfacial ET rates normalized to the coupling strength γ: R^L_{AB}/γ (gray solid line), R^L_{BA}/γ (gray dash), R^R_{AB}/γ (black dash), and R^R_{BA}/γ (black solid line). The following parameters are used: $T = 298$ K, $E_{AB} - \mu = 0.15$ eV, $\lambda = 0.25$ eV. The vertical line indicates the voltage $2V_0$, with V_0 given by Eq. (7).

$$P_{ss}(V) = \frac{P_{eq}(V/2)}{1 + \sigma(V)} \tag{22a}$$

where $V/2$ represents the potential drop across each semi-junction in P_{ss}. In Eq. (22a), it is

$$\sigma(V) = \frac{R^R_{BA}(V)}{R^L_{AB}(V) + R^L_{BA}(V)} \tag{22b}$$

For large enough V, the rate R^L_{BA} of ET to the L metal is negligible and P_{ss} approaches the value $^1/_2$. This stands in contrast to the fact that P_{eq} approaches unity at high overpotential in the voltammetric setup [44]. It is important to understand the behavior of P_{ss} at $V = 2V_0$ (with V_0 given by Eq. (7)). The interface potential difference V_0 determines the condition $R^L_{AB} = R^L_{BA}$ that marks the most rapid dependence on the voltage of the electron exchange at the injection contact (as discussed in Section 3, V_0 has a critical role in the single interface, where, under reversible conditions, it corresponds to the maximum of dP_{eq}/dV, that is, of the current as a function of the overvoltage). For $V = 2V_0$, the inequality $R^R_{BA} >> R^L_{AB} = R^L_{BA}$ holds, hence $\sigma >> 1$ for typical values of λ and $E_{AB} - \mu$, because the threshold voltage for the growth of R^R_{BA} is smaller than that for R^L_{AB} (see Fig. 6 and Supporting Information). Therefore, electrons are much more efficiently delivered from the molecule to the R contact than injected into the molecule by the L electrode, so that the population of the molecular bridge by excess charge is quenched.

We now consider how the above properties of P_{ss} are reflected in the voltage dependence of the bias scan rate u_0 that separates the regimes of reversible and irreversible system response, and in the current over a V cycle. The aim of the analysis is to explain the connection between the properties of the hysteresis loop and the value of the bridge reorganization energy in terms of the λ-dependent evolutions of $P_{ss}(V)$ and $u_0(V)$, by focusing the discussion on V values of special physical relevance.

Inserting into Eq. (21) the expression for P_{ss} in Eq. (22) and writing the analogue of Eq. (6) for P_{ss}, we obtain the condition on the bias sweep rate u for producing reversible current–voltage responses [11]:

$$u << u_0 \equiv \frac{\rho P_{ss}}{|dP_{ss}/dV|} = \frac{R_{AB}}{|dP_{ss}/dV|} = \frac{\rho^2}{\left|\frac{R_{BA}}{R_{AB}}\frac{dR_{AB}}{dV} - \frac{dR_{BA}}{dV}\right|} \tag{23}$$

(to be satisfied at any bias voltage that produces appreciable current). As shown in Fig. 7a, u_0 decreases with increasing reorganization energy of the redox molecular bridge at each V. In particular, at $V = 2V_0$ one finds [11]

$$u_0(2V_0) = \frac{\frac{\gamma}{e}\sqrt{\pi\lambda k_B T}\,\mathrm{erfc}^2\left(\frac{\lambda/2 - eV_0}{\sqrt{\lambda k_B T}}\right)}{\frac{1}{2}\sqrt{\frac{\pi\lambda}{k_B T}}\,\mathrm{erfc}\left(\frac{\lambda/2 - eV_0}{\sqrt{\lambda k_B T}}\right) - \exp\left[-\frac{(\lambda/2 - eV_0)^2}{\lambda k_B T}\right]} \tag{24}$$

which decreases rapidly with increasing λ for $\lambda/2 > E_{AB} - \mu$. Thus, one may expect to obtain I–V curves with more pronounced hysteresis for larger λ, inasmuch as the condition $u << u_0$ becomes farther from being satisfied at common sweep rates (similarly to what happens in the single metal-molecule interface, for which the limiting scan rate was denoted by u_l). However, this is not the case. Fig. 7a shows that the voltage sweep rate threshold for the onset of irreversible I–V response decreases with increasing reorganization energy λ. Therefore, at a given scan rate, the effects of irreversibility should be larger for larger λ. However, in Fig. 8, the hysteresis decreases with increasing λ. In particular, Fig. 8b shows that the maximum width of the hysteresis cycle (normalized to the high-voltage plateau value of the current, which fixes the order of magnitude for appreciable current in the explored V range) decreases with increasing λ.

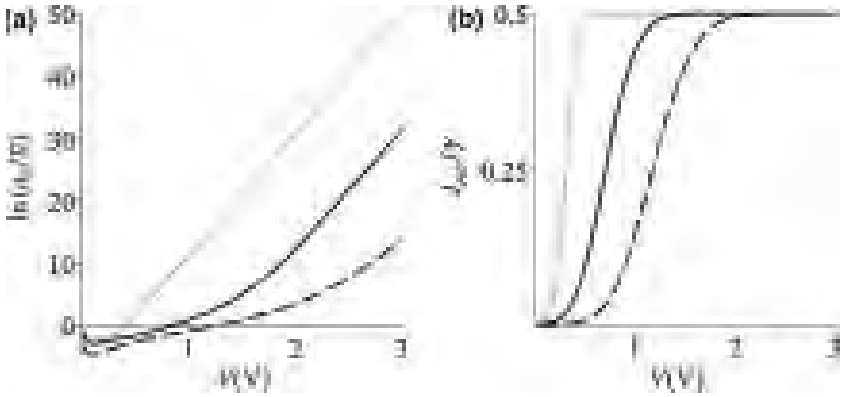

Fig. 7. (a) $\ln(u_0/\overline{u})$ with $\overline{u}/\gamma = 1$ V versus the bias V for a two-state model of metal-molecule-metal junction with $T = 298$ K, $E_{AB} - \mu = 0.15$ eV, and $\lambda = 0$ (solid grey line), $\lambda = 0.25$ eV (black solid line), and $\lambda = 0.5$ eV (black dash). The threshold bias sweep rates are shown starting from 0.01 V; their divergent behavior in close proximity of zero bias (see Supporting Information) is not shown. (b) J_{AB}/γ versus V, plotted for the respective cases in the left panel using the same color code.

To resolve the apparent contradiction between Figs. 7a and 8 we need first to consider that the condition in Eq. (23) predicts the reversibility/irreversibility of the I–V response over the V ranges in which the same current is appreciable. A larger λ entails a wider bias range near $2V_0$ where u_0 is smaller than commonly used scan rates (and thus the system response should show irreversibility), but also a higher threshold bias to obtain detectable current (and therefore, the current is not appreciable for V values in the proximity of $2V_0$, where u_0 is small and irreversibility would otherwise be noticeable; see Figs. 7b and 8a). The dependence of the current at $V = 2V_0$ on the λ value (for any significant λ, that is, $\lambda >> k_BT$) is easily obtained by considering the quenching of the redox center population that results from Eq. (22):

$$J_{AB}(2V_0) = [1 - P_{ss}(2V_0)]R^L_{AB}(2V_0) - P_{ss}(2V_0)R^L_{BA}(2V_0) \cong R^L_{AB}(2V_0) \cong \frac{\gamma}{2}\sqrt{\frac{\pi k_B T}{\lambda}}\exp\left(-\frac{\lambda}{4k_BT}\right) \quad (25)$$

and $J_L(2V_0), J_R(2V_0)$ are of the same order of magnitude as $J_{AB}(2V_0)$, hence also vanish exponentially with λ.

The growth of the current to significant values (namely, to an appreciable fraction of the plateau value $\gamma/2$) occurs at biases for which electrons can be efficiently injected into the redox bridge. The required increase in R^L_{AB}, as V is changed, occurs with maximum rate at the voltage $V_L = 2(V_0 + \lambda/e)$ [10]. Now we show that V_L is a good approximation to the voltage at which the maximum width of the hysteresis loop takes place (see Fig. 8b). Then, we will reconcile the λ -dependencies shown in Figs. 8 and 7a, through the analysis of the limiting scan rate around $V = V_L$, considering that in this voltage range the current is significant and therefore Eq. (23) is the determinant condition to establish the reversibility properties of the I–V response.

For $V > 2V_0$, R^L_{BA} and R^R_{AB} are negligible, while R^L_{AB} and R^R_{BA} determine the charge transfers between molecule and electrodes, with charge accumulation on the molecular bridge and consequent departure of J_L from the steady-state current J_{AB} for large enough u (the analysis is carried out for J_L, but similarly applies to the right-terminal J_R). Thus, inserting ρQ from Eq. (20) into Eq. (17) and using Eq. (22), one obtains

$$J_L - J_{AB} = -\frac{R^L_{AB}}{\rho}(J_L - J_R) = uP_{ss}\frac{dP}{dV} \quad (26)$$

This departure from the steady-state conduction translates into hysteresis over a voltage cycle (note that the sign of $J_L - J_{AB}$ is reversed at the turning point of the bias voltage) and vanishes with decreasing u. For $u << u_0$, P can be replaced by P_{ss} and Eq. (26) becomes

$$\frac{J_L - J_{AB}}{u} = P_{ss}\frac{dP_{ss}}{dV} \quad (27)$$

(both numerator and denominator in the ratio of the left-hand side vanish for $u \to 0$). For different bias cycles with increasing sweep rate, Eq. (27) implies that the first onset of the J_L departure from J_{AB}

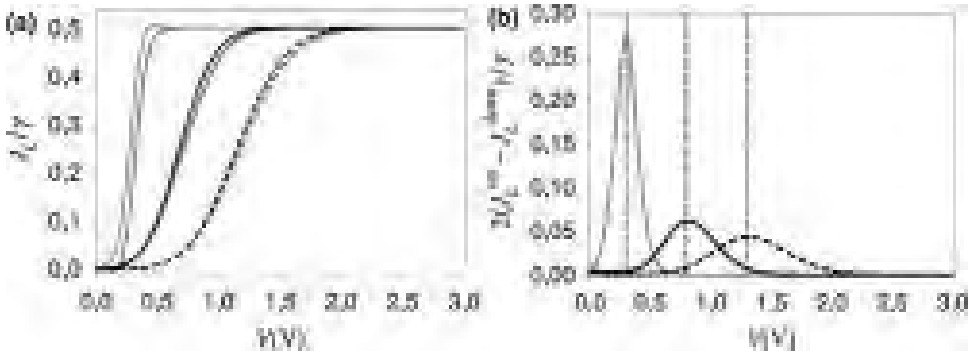

Fig. 8. (*a*) J_L/γ plotted against V according to Eq. (17) for a two-state model junction with $T = 298$ K, $E_{AB} - \mu = 0.15$ eV, $u/\gamma = \frac{1}{3} \cdot 10^{-1}$ V (*e.g.*, $u = 20$ V/s for $\gamma = 300\,s^{-1}$), and $\boldsymbol{\lambda} = 0$ (forward and backward sweeps in grey and pink, respectively), $\boldsymbol{\lambda} = 0.25$ eV (black and red solid lines), $\boldsymbol{\lambda} = 0.5$ eV (black and red dashed lines) Adapted from Ref. [11] (Copyright 2013 American Chemical Society). J_L/γ is here plotted over a larger V range. (*b*) Normalized width of the hysteresis cycle, which is obtained as the difference between the J_L values in the upward (J_L^{up}) and downward $\left(J_L^{down}\right)$ voltage sweeps divided by the J_L plateau value of $\gamma/2$. The vertical dashed lines locate $V = V_L$ for the three $\boldsymbol{\lambda}$ values. A similar analysis can be performed for J_R. (For interpretation of the references to colour in this figure legend, the reader is referred to the web version of this article.)

occurs over a bias range in which P_{ss} is significant and experiences fast evolution, so that P cannot follow P_{ss} as the condition $u << u_0$ begins to fail. Conversely, no hysteresis is expected at sufficiently low and high voltages, for which P_{ss} vanishes or is stationary ($dP_{ss}/dV = 0$) and thus is insensitive to V changes.

On the basis of the above arguments, we search for the bias voltage that corresponds to the maximum width of the hysteresis loop as the maximum of the function of V in the right side of Eq. (27). To simplify the analysis, we consider that the growth of R^R_{BA} occurs around the bias [10] $V_R = 2(-V_0 + \lambda/e) = V_L - 4V_0$, and thus $R^R_{BA} \approx \gamma$ in the voltage range where R^L_{AB} grows if $V_0 = (V_L - V_R)/4 \geq 2s\sqrt{\lambda k_B T}$, where s is any positive real number such that $erfc(x)$ can be neglected for $x \geq s$ (*e.g.*, $R^R_{BA}/\gamma \cong 1$ for $V = V_L$ in Fig. 6). Assuming common V_0 values, and therefore channel energies, that are much larger than k_BT/e [10,45], we can write $P_{ss} \cong R^L_{AB}/\left(\gamma + R^L_{AB}\right)$ and

$$\frac{d}{dV}\left(P_{ss}\frac{dP_{ss}}{dV}\right) = \frac{\gamma\left(\gamma - 2R^L_{AB}\right)}{\left(\gamma + R^L_{AB}\right)^4}\left(\frac{dR^L_{AB}}{dV}\right)^2 + \frac{\gamma R^L_{AB}}{\left(\gamma + R^L_{AB}\right)^3}\frac{d^2R^L_{AB}}{dV^2} = 0 \quad (28)$$

Eq. (28) predicts the first departure of J_L from J_{AB} (which will correspond to the maximum width of the hysteresis loop as u approaches u_0) at $V = V_L$, where R^L_{AB} is $\gamma/2$ and has the maximum rate of change, so that $d^2R^L_{AB}/dV^2 = 0$. This is a very good approximation in all cases shown in Fig. 8. The occurrence of maximum hysteresis at $V = V_L$ is a direct consequence of the predominant role of the charge injection rate R^L_{AB} in determining the evolution of P_{ss}, and hence the transport-mediation properties of the bridge.

V_L increases linearly with λ: $V_L = 2(V_0 + \lambda/e)$. As a consequence, while u_0 decreases with λ at any given V (Fig. 7a), $u_0(V_L)$ increases with λ. In fact, insertion of $P_{ss} \cong R^L_{AB}/\left(R^L_{AB} + \gamma\right)$ and $R^L_{AB}(V_L) = \gamma/2$ into Eq. (23) gives

$$u_0(V_L) \cong \frac{9\gamma}{2e}\sqrt{\pi\lambda k_B T} \quad (29)$$

Indeed, the increase of $u_0(V_L)$ as $\sqrt{\lambda}$ is essentially retained even if R^R_{BA} is appreciably different from γ. In fact, a more accurate expression for u_0 near $V = V_L$ is (see Supporting Information)

$$u_0(V) = \frac{\frac{\gamma}{e}\sqrt{\pi\lambda k_B T}\left[2 + \mathrm{erfc}\left(e\frac{V_L - V}{4\sqrt{\lambda k_B T}}\right)\right]^2}{\frac{2}{\mathrm{erfc}\left(e\frac{V_L - V}{4\sqrt{\lambda k_B T}}\right)}\exp\left[-\frac{e^2(V_L - V)^2}{16\lambda k_B T}\right] - \exp\left[-\frac{e^2(V_L - 4V_0 - V)^2}{16\lambda k_B T}\right]} \quad (30)$$

which gives

$$u_0(V_L) = \frac{\frac{9\gamma}{e}\sqrt{\pi\lambda k_B T}}{2 - \exp\left[-\frac{e^2V_0^2}{\lambda k_B T}\right]} \quad (31)$$

The following picture emerges from the above analysis: if the localization of the transferring charge in the redox bridge is associated with a sufficiently large reorganization energy λ, at $V = 2V_0$ the electron injection rate R^L_{AB} is much smaller than the rate R^R_{BA} of electron delivery to the R electrode. Hence, even though $R^L_{AB}(2V_0) = R^L_{BA}(2V_0)$, which is a critical condition for the voltage-dependent charge dynamics at the L interface, population of the bridge at this voltage is hindered by the high effective channel energy determined by λ. Therefore, no appreciable current is obtained at this voltage, and the λ-dependence of the limiting scan rate $u_0(V)$ below or near $V = 2V_0$ is not reflected in λ-dependent memory effects. At larger voltages, hysteresis occurs if u is close enough to $u_0(V)$ in the spanned bias range. The maximum departure from steady-state conditions is seen near V_L, where $R^L_{AB}(V)$, and hence the bridge population, experiences the maximum rate of change. The value of V_L increases with λ and the evolution of $P_{ss}(V)$ around $V = V_L$ slows down with increasing λ [10]. Therefore, $u_0(V_L)$ increases with increasing λ (see Eq. (23) or (31), and Fig. 7a) and the condition $u << u_0$ is better satisfied for a given bias sweep rate u, which explains the smaller width of the hysteresis loop for larger λ in Fig. 8b.

This state of affairs changes for zero or negligible λ. In this case, assuming $V_0 >> k_BT/e$ (so that the back ET rate R^R_{AB} is negligible at any $V > 0$, as is in all cases considered above), the scan rate separating the reversible and irreversible regimes takes the simple form (see Supporting Information) [46]

$$u_0^{\lambda=0}(V) = \gamma\frac{4k_BT}{e}\left[1 + \exp\left(e\frac{V/2 - V_0}{k_BT}\right)\right] \quad (V > k_BT/e) \quad (32)$$

In particular,

$$u_0^{\lambda=0}(2V_0) = 8\gamma k_BT/e \quad (33)$$

which is four times the value obtained from Eq. (10) for a single interface in the voltammetric context [47]. At this voltage $R^L_{AB} = R^L_{BA} = \gamma/2 \cong R^R_{BA}/2$ (as is easily seen from Eq. (1) of Ref. [10]), so that $J_L^{\lambda=0} \approx J_{AB}^{\lambda=0} \cong \gamma/4$. Thus, for negligible reorganization energy, hysteresis appears in the I–V response of a junction at sweep rates comparable to those that cause irreversible behavior in the ET dynamics at the single interface.

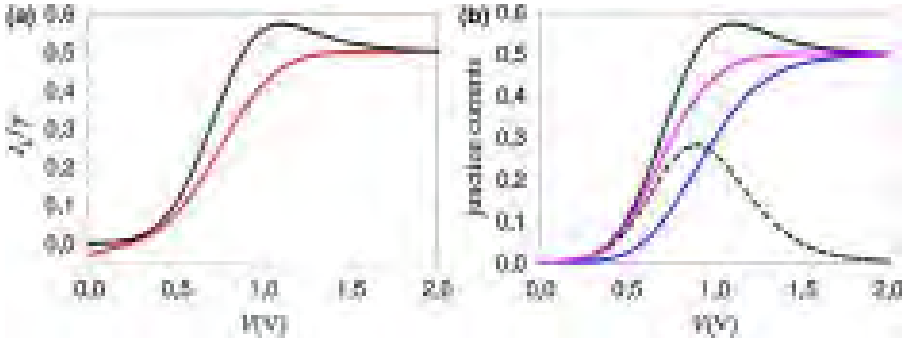

Fig. 9. (a) J_L/γ plotted against V using Eq. (17) with model parameters $T = 298$ K, $E_{AB} - \mu = 0.15$ eV, $\boldsymbol{\lambda} = 0.25$ eV, and $u/\gamma = 0.4$ V. The upward and downward bias sweeps are represented in black and red, respectively. (b) Dimensionless steady-state current J_{AB}/γ (pink), L terminal current J_L/γ, R terminal current J_R/γ (blue), and "leakage" current $dP/dt = udP/dV$ (black dash) over the forward bias sweep. (For interpretation of the references to colour in this figure legend, the reader is referred to the web version of this article.)

In concluding this section, we note that the charge accumulation on the molecule during a fast voltage sweep (namely, $u \gtrsim u_0$ over a significant voltage range) leads to transient NDR in the I–V characteristic if dP/dt becomes comparable to the steady state and terminal currents (see Figs. 9a–b). This is visible in Fig. 8a for $\lambda = 0$ and evident in Fig. 9a for $\lambda \neq 0$ at a higher sweep rate. During the forward sweep, the evolution of the redox site population P accumulates a delay with respect to $P_{ss}(V)$; so, $Q = P - P_{ss} < 0$.

The missing charge in the redox site quantified by Q corresponds to a decrement $(R^R_{AB} + R^R_{BA})Q$ in the R terminal current, as expressed by Eq. (18). In contrast, the surplus of electronic charge required from the L contact to establish the equilibrium interfacial ET dynamics at a given V implies an additional current $-(R^L_{AB} + R^L_{BA})Q$ at the left terminal, as described by Eq. (17). The resultant rate $dP/dt = -(R_{AB} + R_{BA})Q$ of population of the molecular redox site causes transient NDR during the forward voltage sweep, while, as observed in various experiments (*e.g.*, see Ref. [48]), no transient NDR occurs during the backward sweep, where $Q > 0$ (thereby, $dP/dt < 0$) amounts to $J_L < J_{AB}$ rather than to an overshoot of J_L beyond J_{AB}. The present analysis provides a simple explanation of (transient) hysteretic NDR in terms of irreversible charge storage in and release from the molecular bridge, without additional assumptions [48] on the relative rates of molecular reduction and oxidation in the forward and backward sweeps. The quantitative results of our formulation (for example, the plateau in the current response at high voltages) reflect the use of a two-state hopping junction model, but the proposed basic mechanism for hysteretic NDR may be the one at play in experiments such as those of Ref. [48].

Another irreversible behavior appears in the backward sweep: a residual negative L-terminal current at $V = 0$, where P is still appreciable and, since $R^L_{BA} >> R^L_{AB}$ (for $E_{AB} - \mu >> k_BT$), Eq. (17) leads to the current $J_L \cong -PR^L_{BA}$ (*i.e.*, the molecular bridge discharges to the L electrode). The real experiment will measure a current that may be neither J_L nor J_R, and will be closer to J_L or J_R depending on the junction architecture. Yet even for cases in which the current is well approximated by the average of eJ_L and eJ_R, the non-steady-state terms in Eqs. (17) and (18) do not cancel each other out, because R^L_{AB} and R^R_{BA} grow at different voltages. Therefore, also in such cases the present model leads to the occurrence of transient NDR.

5. Conclusions

In this work, we employed a two-state model of redox molecules to build a consistent description and characterization of different irreversibility effects such as the distortion and relative shift [1] of the current peaks in cyclic voltammograms, and the occurrence of hysteresis [49] and transient hysteretic NDR [48] in the current–voltage response of redox molecular conduction junctions. Table 1 summarizes the main results of this work, which may be used to interpret electrochemical data and the current-bias voltage responses of redox molecular junctions, under conditions of reversible and irreversible operation.

The local stability of the states of a redox molecular system [49] allows conduction regimes amenable to description in terms of Marcus-type ET processes [14,15]. In such conditions, the reorganization energy that characterizes the response of the molecular environment to the ET plays an important role in making the transitions between redox states slow enough that the measured current does not follow adiabatically the external bias in sufficiently fast voltage scans. This mechanism for irreversibility operates in conduction systems with either one or two metal-molecule interfaces. Therefore, before investigating the occurrence of hysteresis in the current–voltage responses of metal-molecule-metal junctions, we analyzed the charge dynamics at a single interface. In this analysis, we related the reorganization energy to the threshold scan rate for the onset of irreversibility, on the one hand, and to the appearance of this irreversibility in cyclic voltammetry, on the other.

Understanding the different appearance of irreversibility (that is, memory effects) in the responses of single and double (junction) metal-molecule interfaces to an external voltage requires understanding of the different voltage-dependences of the redox center population in the two cases. In the junction, the adjustment of the average redox state (*i.e.*, the average occupation of the molecular bridge by the excess transferring charge) to the changing bias voltage is determined by the competition of the ET rates at both interfaces, which are characterized by different threshold voltages [10]. As compared to the case of a single interface, this translates into a more involved dependence of the minimum bias-scan rate for occurrence of irreversibility on the reorganization energy. Investigating this dependence, we found that the potential difference at the injection interface is determinant to produce both appreciable current and memory effects.

Table 1
Summary of the main results of this work. The equations from Ref. [11] exploited in the present study are also mentioned. The redox molecule is modeled as a two-state system and cyclic voltammetry of diffusionless [27,12] electrochemical systems is investigated. In the voltammetry setup, it is considered that the peak potential corresponds to an irreversible (namely, unidirectional) electrode reaction for large enough scan rate [39].

	Equation
Single metal-molecule interface (voltammetric setup)	
Condition on the scan rate for reversible/irreversible behavior (Ref. [11] and this work)	(6)
Upper bound for scan rates that lead to reversible behavior [11]	(9)
Overpotential-dependent scan rate threshold for reversible/irreversible behavior [11]	(10)
Peak potential at large scan rates	(13)
Asymptotic expression for the peak potential	(14)
Strategy to find the reorganization energy from peak potential measurements	(15,16)
Double metal-molecule interface (junction)	
Condition on the sweep rate for reversible/irreversible behavior [11]	(23)
Sweep rate threshold at the critical voltage for the electron injection dynamics [11]	(24)
Sweep-rate dependent deviation of the current from steady-state	(27)
Bias for hysteresis first-appearance and maximum	(28)
Sweep rate threshold at the voltage threshold of the injection rate	(31)
Bias-dependent sweep rate threshold for zero reorganization energy	(32)

In particular, while larger λ produces more significant distortion of a cyclic voltammogram from its ideal shape, the width of hysteresis loop in the current-voltage response of a junction can even decrease with increasing λ (*e.g.*, see Fig. 8). This results from the λ-dependent mismatch between the bias ranges where the current may not follow adiabatically the changing bias at common sweep rates and where the electron injection rate, and thus the current, becomes appreciable.

The expression of the threshold bias-sweep rate for irreversibility (u_0) shows that the metal-molecule coupling strength γ also plays a role in determining appreciable memory effects at feasible sweep rates. Using sufficiently large redox molecules, the electronic coupling between redox center and electrode can be sufficiently small to lead to appreciable non-steady state behavior at common sweep rates, but then an array with many redox molecules may be needed to produce an appreciable current. Ultimately, redox molecules whose operation involves at least two charge-transport channels of different efficiency appear to be a critical ingredient to implement single-molecule devices, where significant current flows through an efficient transport channel and reflects a redox state switching (the other channel) on the time scale of the observation [11]. The concept of two interacting transport channels has been used in recent experiments to study the dynamics of the slow channel [50], which opens the way to direct experimental investigation of the models studied in this work and in Refs. [10] and [11].

Recent experimental studies [51,34] show that currents through some solid state molecular junctions are not considerably affected by the presence or absence of redox centers. In particular, it is shown that [34] the order of magnitude of the currents via cytochrome c and human serum albumin–hemin proteins does not change after removal of the iron, while the porphin is found to be more critical for efficient conduction in solid state conditions. However, it is important to note that: (a) the current is reduced by a significant fraction of the observed range after iron removal (for example, see Fig. 2b in Ref. [34]), which points to possible significant interaction between the slow transport channel (which involves Fe) and the efficient transport channel that may involve the porphin in the system with Fe. (b) The role of the Fe center may become very important in bias sweeps sufficiently fast to produce memory effects in the current–voltage response. Then, (*e.g.*, if we suppose that the conductance of the protein with Fe in one of the oxidation states is similar to that of the Fe-free protein) significant hysteresis may be determined by the Fe-involving slow transport channel under irreversible operation conditions, that is, when the sweep rate is so fast that the average redox state of Fe is not able to adapt quasi-statically to the changing voltage. (c) The observed strong effect of Fe removal on the cyclic voltammograms of Ref. [34] are not in contrast with the preserved order of magnitude of the current, because the latter is mainly determined by the fast transport channel. (d) The interaction between the electrons involved in the two channels may be screened and thus widely reduced in the large molecular systems of Ref. [34] (χ interaction parameter in Ref. [11]), therefore not leading to significant effect of the Fe (hence, of its oxidation state) on the threshold bias voltage for the onset of significant current via the fast channel (yet, some small effect may be present in Fig. 2 of Ref. [34]). (e) The apparent discrepancy between the effects of the iron center on the cyclic voltammograms and current–voltage characteristics of Ref. [34] might be justified using the models presented in this work. In this regard, we note that our theoretical analysis in this work was applied to a range of reorganization energy values that overlaps with that expected in the absence of bulk polar solvent. We think that these considerations foster future experimental investigations that can give great relevance to the present analysis in the fields of electrochemical and molecular electronics.

Acknowledgements

This research was supported by the Israel Science Foundation, the Israel-US Binational Science Foundation (grant no. 2011509) and the European Research Council under the European Union's Seventh Framework Program (FP7/2007–2013; ERC grant agreement no. 226628).

Appendix A. Analytical expression of the peak (over)potential from Eq. (12)

To derive Eq. (13), we first notice that for $x \geq 0$ the error function can be written as [52]

$$\mathrm{erf(x)} = 1 - \left(a_1\theta + a_2\theta^2 + a_3\theta^3\right)\exp(-x^2) + \Delta(\mathrm{x}),$$
$$\theta = \frac{1}{1+px} \quad |\Delta(x)| \leq 2.5\cdot 10^{-5} \tag{A1}$$

with the numerical coefficients a_1, a_2, a_3, and p defined as above. Neglecting the error $\Delta(x)$, inserting $\mathrm{erfc}(x) = 1 - \mathrm{erf}(x)$ into Eq. (12a), taking the square root and multiplying by $\exp(x^2)$, we obtain

$$a_1\theta + a_2\theta^2 + a_3\theta^3 = \frac{a_1p^2x^2 + (2a_1 + a_2)px + 1}{(1+px)^3} = 2D\exp(x^2/2) \cong D(2+x^2) \tag{A2}$$

for $D \lesssim 1$ given by Eq. (13e). In the rightmost side of Eq. (A2) we neglected terms of forth and higher order in x, which is allowed for x sufficiently smaller than unity [53]. Multiplying both sides of Eq. (A2) by $(1+px)^3$, neglecting again terms of forth and higher order in x and rearranging, we obtain the cubic equation

$$x^3 + Ax^2 + Bx + C = 0 \tag{A3}$$

where A, B and C are given by Eq. (13c). Solution of this equation by Cardano's method [54] yields

$$x = \sqrt[3]{-\frac{\nu}{2} + \sqrt{\frac{\nu^2}{4} + \frac{\eta^3}{27}}} + \sqrt[3]{-\frac{\nu}{2} - \sqrt{\frac{\nu^2}{4} + \frac{\eta^3}{27}}} - \frac{A}{3} \text{ for } \frac{\nu^2}{4} + \frac{\eta^3}{27} \geq 0 \tag{A4a}$$

as it is in the cases of Figs. 2 and 3, or

$$x_k = 2\sqrt{-\frac{\eta}{3}}\cos\left[\frac{1}{3}arccos\left(-\frac{\nu}{2}\sqrt{-\frac{\eta^3}{27}}\right) + \frac{k2\pi}{3}\right]$$
$$k = 0, 1, 2, \text{ for } \frac{\nu^2}{4} + \frac{\eta^3}{27} < 0 \tag{A4b}$$

Eqs. (12b) and (A4a) lead to Eq. (13a) with the coefficients defined in Eq. (13c). On the other hand, for $x \leq 0$, we exploit the fact that erf is an odd function of its argument; so in place of Eq. (A1) we write

$$\mathrm{erf}(-x) = 1 - \left(a_1\vartheta + a_2\vartheta^2 + a_3\vartheta^3\right)\exp\left(-x^2\right) + \Delta(-x),$$
$$\vartheta = \frac{1}{1-px}, \quad |\Delta(-x)| \leq 2.5\cdot 10^{-5} \tag{A5}$$

Inserting the corresponding expression of $\mathrm{erfc}(x)$ into Eq. (12a), taking the square root of both sides of the equation, multiplying by $\exp(x^2)$, and neglecting terms of forth or higher order in x, we obtain again Eq. (A3), but with the coefficients given by Eq. (13d). Finally, the solution has the form of Eq. (A4).

At sufficiently high scan rates, it is $x < 0$ at the peak potential and Eq. (12) yields

$$4D^2 = \mathrm{erfc}^2(x)\exp(x^2) \cong 4\exp(x^2) \tag{A6}$$

Inserting the expressions of D (here not limited to be less than unity) and x, taking the natural logarithm and then the square root of both sides, one obtains Eq. (14) from

$$\sqrt{\ln\left(\frac{e}{2\gamma\sqrt{\pi\lambda k_B T}}u\right)} \cong \frac{|\lambda + E_{AB} - \mu - eV|}{2\sqrt{\lambda k_B T}} \tag{A7}$$

from which Eq. (14).

References

[1] C. Léger, P. Bertrand, Chem. Rev. 108 (2008) 2379–2438.
[2] T. Albrecht, Nat. Commun. 3 (2012) 829.
[3] N.F. Polizzi, S.S. Skourtis, D.N. Beratan, Faraday Discuss. 155 (2012) 43–62.
[4] A. Okamoto, K. Hashimoto, K.H. Nealson, R. Nakamura, Proc. Natl. Acad. Sci. U.S. A. 110 (2013) 7856–7861.
[5] A. Nitzan, Annu. Rev. Phys. Chem. 52 (2001) 681–750.
[6] N.J. Tao, Nature Nanotechnol. 1 (2006) 173–181.
[7] M. Di Ventra, Electrical Transport in Nanoscale Systems, New York, Cambridge University Press, 2008.
[8] P. Petrangolini, A. Alessandrini, L. Berti, P. Facci, J. Am. Chem. Soc. 132 (2010) 7445–7453.
[9] H.M. Wen, Y. Yang, X.S. Zhou, J.Y. Liu, D.B. Zhang, Z.B. Chen, J.Y. Wang, Z.N. Chen, Z.Q. Tian, Chem. Sci. 4 (2013) 2471–2477.
[10] A. Migliore, A. Nitzan, A C S Nano 5 (2011) 6669–6685.
[11] A. Migliore, A. Nitzan, J. Am. Chem. Soc. 135 (2013) 9420–9432.
[12] By "diffusionless" we mean that the ET processes described below are the only rate processes in the model.
[13] R.W. Gurney, Proc. R. Soc. Lond. A 134 (1931) 137–154.
[14] R.A. Marcus, Ann. Rev. Phys. Chem. 15 (1964) 155–196.
[15] R.A. Marcus, J. Chem. Phys. 43 (1965) 679–701.
[16] N.S. Hush, Electrochim. Acta 13 (1968) 1005–1023.
[17] W. Schmickler, Electrochim. Acta 20 (1975) 137–141.
[18] C.E.D. Chidsey, Science 251 (1991) 919–922.
[19] M.J. Honeychurch, Langmuir 15 (1999) 5158–5163.
[20] K.B. Oldham, J.C. Myland, J. Electroanal. Chem. 655 (2011) 65–72.
[21] A. Migliore, A. Nitzan, J. Electroanal. Chem. 671 (2012) 99–101.
[22] A.M. Kuznetsov, I.G. Medvedev, Phys. Rev. B 78 (2008) 153403.
[23] A.M. Kuznetsov, I.G. Medvedev, J. Ulstrup, J. Chem. Phys. 131 (2009) 164703.
[24] N.J. Tao, J. Mater. Chem. 15 (2005) 3260–3263.
[25] Z.H. Li, Y.Q. Liu, S.F.L. Mertens, I.V. Pobelov, T. Wandlowski, J. Am. Chem. Soc. 132 (2010) 8187–8193.
[26] A. Migliore, P. Schiff, A. Nitzan, Phys. Chem. Chem. Phys. 14 (2012) 13746–13753.
[27] E. Laviron, J. Electroanal. Chem. 101 (1979) 19–28.
[28] G.G.H.G. Láng, Electroanalysis 11 (1999) 905–906.
[29] M.J.R. Honeychurch, G. A, Electroanalysis 11 (1999) 907–908.
[30] Using a language familiar to electrochemistry, the overpotential refers the potential difference between the working electrode and the reference electrode (which determines the potential at the redox centers) to its equilibrium value in the absence of external voltage.
[31] A.P. Brown, F.C. Anson, J. Electroanal. Chem. 92 (1978) 133–145.
[32] A. Nitzan, Chemical dynamics in condensed phases, Oxford University Press, Oxford, 2007, pp. 610.
[33] S. Sek, B. Palys, R. Bilewicz, J. Phys. Chem. B 106 (23) (2002) 5907–5914.
[34] N. Amdursky, D. Ferber, I. Pecht, M. Sheves, D. Cahen, Phys. Chem. Chem. Phys. 15 (2013) 17142–17149.
[35] X.S. Zhou, L. Liu, P. Fortgang, A.S. Lefevre, A. Serra-Muns, N. Raouafi, C. Amatore, B.W. Mao, E. Maisonhaute, B. Schöllhorn, J. Am. Chem. Soc. 133 (2011) 7509–7516.
[36] E. Laviron, J. Electroanal. Chem. 39 (1972) 1–23.
[37] J. Hirst, F.A. Armstrong, Anal. Chem. 70 (1998) 5062–5071.
[38] D. Suwatchara, N.V. Rees, M.C. Henstridge, E. Laborda, R.G. Compton, J. Electroanal. Chem. 665 (2012) 38–44.
[39] J.C. Myland, K.B. Oldham, Electrochem. Commun. 7 (2005) 282–287.
[40] J.M. Hale, J. Electroanal. Chem. 19 (1968) 315–318.
[41] L. Tender, M.T. Carter, R.W. Murray, Anal. Chem. 66 (1994) 3173–3181.
[42] Eq. (20) is the same as Eq. (23) in Jauho, A.-P.; Wingreen, N. S.; Meir, Y. Phys. Rev. B 1994, 50, 5528–5544, except for the sign convention for J_R, and the expression of dP/dt in terms of Marcus ET rates and Q in this work.
[43] Z. Li, B. Han, G. Mészáros, I. Pobelov, T. Wandlowski, A. Blaszczyk, M. Mayor, Faraday Discuss. 131 (2006) 121–143.
[44] Particularly significant is the case of resonance, at zero V, between the metal Fermi level and the molecular level: $E_{AB} = \mu$. In this case, the forward ET rates at the two interfaces are equal (while the backward ET rates are negligible for positive V values that produce appreciable current) and $P = P_{ss} = 1/2$ while V is changed. Thus, when the model is applicable, no hysteresis is seen in the I–V response of the junction irrespective of the V scan rate. In contrast, $E_{AB} = \mu$ is not a special case for the response of a voltammetric system.
[45] M. Galperin, M.A. Ratner, A. Nitzan, Nano Lett. 5 (2005) 125–130.
[46] The specification $\lambda = 0$ is added to u_0, to distinguish this special case from the general case with nonzero λ.
[47] A factor of two results from the contribution of the ET rates at both contacts to the effective rate ρ that appears in the denominator of P_{ss}. In other words, the electron delivery to the R contact reduces the rate of charge storage in the molecular redox site with changing V. Another factor of two is consequence of the fact that only half of the applied bias voltage appears at the single interface, which halves the change rate of the molecular occupation probability with V.
[48] R.A. Kiehl, J.D. Le, P. Candra, R.C. Hoye, T.R. Hoye, Appl. Phys. Lett. 88 (2006) 172102.
[49] M. Galperin, M.A. Ratner, A. Nitzan, A. Troisi, Science 319 (2008) 1056–1060.
[50] R. Arielly, M. Vadai, D. Kardash, G. Noy, Y. Selzer, J. Am. Chem. Soc. 136 (2014) 2674–2680.
[51] I. Ron, L. Sepunaru, S. Itzhakov, T. Belenkova, N. Friedman, I. Pecht, M. Sheves, D. Cahen, J. Am. Chem. Soc. 132 (2010) 4131–4140.
[52] C. Hastings Jr., Approximations for Digital Computers, Princeton University Press, Princeton, N.J, 1955.
[53] Note that, even for $x = 0.8$, the fourth-order term in the Taylor expansion of the exponential is about 0.05, that is 0.16 of the second-order term.
[54] G. Cardano, Artis Magnae, Sive de Regulis Algebraicis, Nuremberg, 1545.